Higher-order accurate finite volume discretization of Helmholtz equations with Pollution Effects Reductions

Yaw Kyei

Department of Decision Sciences, North Carolina Central University Durham, NC 27707, ykyei@nccu.edu

Kossi Edoh

Department of Mathematics, North Carolina A & T State University Greensboro, NC 27411, kdedoh@ncat.edu

Abstract

Higher-order accurate finite volume schemes are developed for Helmholtz equations in two dimensions. Through minimizations of local equation error expansions for the flux integral formulation of the equation, we determine quadrature weights for the discretization of the equation. Collocations of local expansions of the solution and the source terms are utilized to formulate weighted quadratures of all local compact fluxes to describe the equation error expansion within the computational domain. In using the source term distribution to account for fluxes along all compact directions about each grid point as the centroid of a local control volume, the right minimizing quadrature weights are determined and optimized for stability and uniform higher-order convergence. As a result, the resulting local residuals form more complete descriptions of the wave number k and the complexities of the associated pollution effects. The leading terms of the residual errors are optimized for pollution effects reductions to ensure stability and robust convergence of the resulting schemes. Numerical results and analysis of the schemes demonstrate the effectiveness of the methodology.

Introduction

Numerical methods for simulating the Helmholtz equations have continued to receive significant attention as reported in the literature [7,28] addressing the quality of the numerical solutions due to pollution effects associated high wave numbers. As clearly described [28], there have been a lot of published work utilizing the finite element method [1,7], the finite difference method [30], the boundary element method [15] as well as the spectral element method [17] addressing the problem of the pollution effects of the numerical solution of the Helmholtz equation. The compact finite difference method has also been utilized for the Helmholtz equation [5] as well as for general elliptic equations [20,24,26] since they achieve high-order accuracies without significant increase in the size of the resulting system matrices.

The use Taylor series expansions to develop numerical schemes is not new and in [25], the traditional fourth order scheme for the Poisson equation on the compact nine-point stencil was derived.

The technique has been extended to develop higher-order compact schemes [12] and for other application problems [8,13,30]. Basically, the univariate series expansion is utilized to derive the finite difference approximations of the individual terms of the differential equation and then coupled to obtain the numerical schemes for multi dimensions. Associated truncation errors are formulated to assess the accuracy of the schemes.

In [11], local multivariate expansions are utilized to develop higher-order discretizations for the Poisson equations in 3D. First, local expansions for the solution and the source terms are utilized to formulate the equation error for discretizing the equation using weight parameters for the grid functions in characterizing the derivatives in the equation in an undetermined fashion. By determining the parameters to annihilate the leading coefficients of the error, the parameter-based fourth order compact schemes are derived. In [10], the approach was extended to develop a space-time finite volume differencing framework for effective higher-order accurate discretizations of parabolic equations. In [11], the traditional fourth order compact scheme [25] is recovered as a parameterized version of the general parameter-based discretization of the Poisson equation. Numerical experiments show that other parameter-valued schemes are much more stable and robust than traditional fourth order compact scheme. In [10], several higher-order discretizations are constructed for the parabolic equation including a new scheme on the Crank-Nicholson stencil which is fourth order accurate along a parabolic space-time curve. In these cases, the resulting local residual errors are utilized to optimize the resulting schemes to achieve uniform computational convergence rates as reported.

In this paper we present higher-order finite volume discretizations of the Helmholtz equations in two dimensions with a framework for effective reductions in the pollution effects associated with the numerical simulations of the equations. The schemes are designed based on using a multivariate series expansions to approximate local manifolds of the solution to ensure a more accurate charaterization of local fluxes. Generalized weighted quadratures of the local solution expansions are utilized to formulate local equation error expansions based on flux integral formulations of the equation in order to capture all local compact fluxes and preserve operator properties of the equation. The weighted quadrature descriptions express the approximation of the divergence of flow about each grid point on the computational domain and offers the right framework to allow for effective higher accuracies and ensure a more uniform higher-order convergence. Considering flux divergence at each grid point, the interconnections to neighboring points may be expanded to improve local flux modeling within the computational domain. Therefore, as more neighboring grid points are included in this framework more robust higher accuracies are achieved.

The local equation residual from the flux differencing within the balanced formulation of the equation includes all directions of grid points instead of just coordinate directions as in traditional finite difference schemes [12,22,25]. This formulation exhaustively captures the sum of the approximation errors as the local equation error residual. The formal error is then minimized by eliminating much of the terms coupled with the wave numbers in the error to improve consistency, stability, and increase the order of the resulting schemes as much as possible. The extent and effectiveness of the resolution of the couplings of the wave number depend on the number of grid points utilized locally. Numerical results and analysis of the schemes demonstrate the effectiveness of the methodology on stability and accuracy for higher wave numbers.

Consider the elliptic boundary value problem

$$-\operatorname{div}(\mu \nabla u) + c u = q, \quad x \in \Omega \tag{1.1}$$

$$-\operatorname{div}(\mu \nabla u) + c u = q, \quad x \in \Omega$$

$$\mu \frac{\partial}{\partial \nu} u + \alpha u = g, \quad x \in \Gamma$$
(1.1)

where Ω is an open regular bounded domain in \mathbb{R}^2 with v as the outward normal to the smooth boundary Γ and assume that μ , f, c, α , g are sufficiently smooth.

To obtain higher computational efficiencies and performances desired of higher-order methods, a complete characterization of the local equation error within the computational domain must be formulated using the balanced flux integral formulation the equation. We therefore base our approach and methodology on multivariate Taylor series expansion to approximate the solution locally in order to more accurately represent and account for all local compact fluxes. To conserve the properties of the equation and be applicable to a range of applications, we use the finite volume idea [20] of conservative integral representation of the equation. However, we adopt grid-point centered control volumes in this formulation to reflect the series expansion of the local manifold containing the solution. Adopting a uniform distribution of grid points on the control volume ensures that symmetric system matrices are achieved for the resulting schemes.

The contributions of this paper include:

- A systematic framework based on the finite volume methodology is described for a general elliptic equation which allows for using local fluxes in discretizing the more balanced integral formulation of the equation. Adaptive ways to utilize more local as well as nonlocal fluxes are supported and all fluxes are accounted for by the framework to ensure conservation within the computational domain.
- The residual errors for the resulting schemes are more completely and accurately determined through optimizations of the equation error expansion to ensure uniform higher-order convergence rates.
- Effective ways to optimize sensitivities of resulting numerical models to coefficients of the differential equation.
- The design supports the use of other vertex-centered control volumes [26] to develop efficient higherorder accurate methods.

The paper is organized as follows: In Section 2 we present the framework of the method by describing the discretization for a general elliptic equation in flux divergence form locally in ². In Section 3, we apply the method to develop new efficient higher-order schemes for the Helmholtz equations in two dimensions. We present the resulting fourth order schemes in Section 4 and illustrate the pollution effects for the fourth order schemes due to high values of the wave number k. We further illustrate the effectiveness of the new schemes in reducing the indefiniteness associated with Helmholtz equation in the fourth order schemes and consistency improvements in Section 4.1. Then the extension to the sixth order schemes are described in Section 4.2 and numerical results demonstrating the accuracies of the methods are illustrated in Section 5. Conclusions are presented in Section 7.

The finite Volume Discretization Framework

We describe the finite volume differencing discretization method for the elliptic boundary value problem

$$-\nabla \cdot (\kappa \nabla u) + c u = q, \quad \text{in } \in \Omega$$
 (2.1)

$$u = g, \quad \text{on } \in \Gamma$$
 (2.2)

where Ω is a bounded domain in \mathbb{R}^2 with a smooth boundary Γ . We assume that $\kappa \in L^{\infty}(\Omega)$ and is positive and the source $q \in L^2(\Omega)$.

To develop a higher-order accurate discretization for (2.1) with robust computational accuracy, the discretization framework must effectively account for all local compact fluxes to describe the diffusion effectively within the computational domain. That is, the framework must be conservative of all local fluxes [6] required for consistent and robust higher-order accuracies. We therefore formulate the equation (2.1) over local control volumes which can provide the needed support for local fluxes to neighboring grid points rather than independently in univariate Cartesian coordinate directions [21] as in traditional finite difference formulations.

We first write the integral formulation of the equation (2.1) as

$$-\int_{\Omega} \nabla \cdot \kappa \nabla u \, dv + \int_{\Omega} c \, u \, dv = \int_{\Omega} q \, dv \tag{2.3}$$

where dv = dxdy in \mathbb{R}^2 . By the divergence theorem, equation (2.3) is rewritten into the flux integral balanced form as

$$-\oint_{\partial\Omega} \kappa \nabla u \cdot \nu \ dS + \int_{\Omega} c \, u \, dv = \int_{\Omega} q \, dv \tag{2.4}$$

where v is the unit outward normal to the boundary S of the domain Ω .

Now, consider the domain Ω partitioned into control volumes where each control volume is identified by its centroid mesh point and a distribution of neighboring mesh points as in Figure 1. A uniform distribution of grid points is utilized for this work but the approach is applicable for a non-uniform distribution as well. A combination of uniform distribution for regular grid points and non-uniform distribution for irregular grid-points may be adopted for handling discretizations on non-rectangular domains [8]. The grid-point clouds for neighboring control volumes overlap [27] to create interlocking configurations which help to capture and track local fluxes effectively on the computational domain necessary for higher level of conservation and robust higher-order rates of convergence.

We thus describe (2.4) about the centroid of each control volume \mathbf{Q}_h by

$$-\oint_{\partial \mathbf{Q}_h} \kappa \nabla u \cdot \nu_h \, dS_h + \int_{\mathbf{Q}_h} c \, u \, dv = \int_{\mathbf{Q}_h} q \, dv \tag{2.5}$$

where v_h is the unit outward normal vector to S_h which is the boundary of \mathbf{Q}_h . The equation (2.5) represents the conservation of u about the centroid of the control volume such that variations in the source distributions

within the control volume are compensated for by the local diffusive fluxes through the boundary S_h [9]. Thus, the distribution of u within the control volume \mathbf{Q}_h is completely determined by the sum of all diffusive radial fluxes about the centroid and the corresponding source distribution. Hence, the associated equation error, E(u), about the centroid is given by

$$E(u) = -\oint_{\partial \mathbf{Q}_h} \kappa \nabla u \cdot \nu_h \, dS_h - \int_{\mathbf{Q}_h} c \, u \, dv \, - \int_{\mathbf{Q}_h} q \, dv \, = 0. \tag{2.6}$$

where $\mathbf{Q}_h = [x_m - h, x_m + h] \times [y_n - h, y_n + h]$ is a typical control volume with centroid $X_0(x_m, y_n)$, as illustrated by Figure 1. The control volume \mathbf{Q}_h illustrated with centroid X_0 and a compact cloud of quadrature points $X_1(x_m + h, y_n)$, $X_2(x_m + h, y_n + h)$, $X_3(x_m, y_n + h)$, $X_4(x_m - h, y_n + h)$, $X_5(x_m - h, y_n)$, $X_6(x_m - h, y_n - h)$, $X_7(x_m, y_n - h)$, and $X_8(x_m + h, y_n = h)$ overlaps with control volumes centered on all these compact quadrature points.

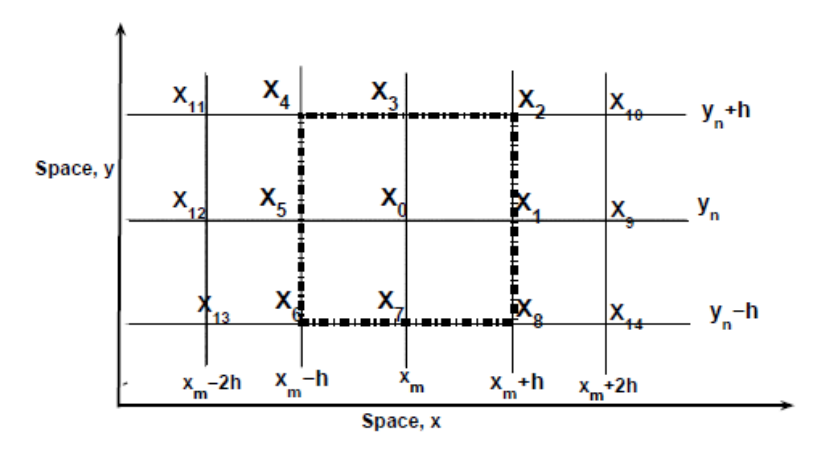


Figure 1: Control volume Q_h in \mathbb{R}^2 with local uniform compact cloud of quadrature points with $X_0(x_m, y_n)$ as the centroid

By using a finite number of quadrature points to approximate the local equation error, the discrete version of (2.6) is therefore nonzero. In fact, we approximate local diffusive fluxes about the centroid of the control volume by a generalized weighted quadrature of the radial fluxes to the neighboring quadrature points by

$$\int_{\partial \mathbf{Q}_h} \kappa(u) \nabla u \cdot \nu_h \, dS_h \approx \sum_{\partial \mathbf{Q}_h} \kappa(u_0) \nabla u \cdot \nu_h \approx \kappa(u_0) \sum_{i=1}^{n_i} w_i (u_i - u_0)$$
 (2.7)

where n_i is number of quadrature points, w_i is the collocation weight for the local directional flux, $\nabla u \cdot v_{hi}$ = $(u_i - u_0)$ along the radial direction v_{hi} toward location of u_i . The number of quadrature points forming the desired local distribution is part of the available degrees of freedom, which may be increased to improve local accuracy by incorporating more local and nonlocal fluxes [3].

Based on the adopted set of neighboring quadrature points, the quadrature formulation of (2.4) about the centroid of the control volume becomes

$$-\kappa(u_0) \sum_{\partial Q_h} W_i (u_i - u_0) - \sum_{Q_h} w_i u_i = \sum_{Q_h} v_i q_i, \qquad (2.8)$$

where $\kappa(u_0)$ is an averaging value of $\kappa(u)$ about the centroid. Clearly, the framework as described in (2.8) allows for both regular and non-regular distribution of quadrature points locally about each centroid and adaptively.

For a more complete modeling of the local equation error (2.12) in all radial directions, we adopt a local multivariate Taylor series expansion for u about each centroid (x_0, y_0) by

$$\phi(x_0 + x, y_0 + y) = \sum_{m=0}^{\infty} \sum_{i+j=m} \frac{C(m, i)}{m!} \frac{\partial^m \phi}{\partial x^i \partial y^j} (x_0, y_0) x^i y^j$$
(2.9)

where φ is sufficiently smooth and locally defined everywhere such that

$$\phi(x_0, y_0) = u(x_0, y_0)
\frac{\partial^m \phi}{\partial x^i \partial y^j}(x_0, y_0) = \frac{\partial^m u}{\partial x^i \partial y^j}(x_0, y_0).$$

Consequently, we define the local source term by

$$f(x_0 + x, y_0 + y) = -\Delta_{\kappa} \left(\sum_{m=0}^{\infty} \sum_{i+j=m} \frac{C(m, i)}{m!} \frac{\partial^m \phi}{\partial x^i \partial y^j} (x_0, y_0) x^i y^j \right)$$
(2.10)

where Δ_{κ} is the local differential operator description of (2.1) with unique characteristics of the equation [16] such that

$$f(x_0, y_0) = q(x_0, y_0) = \Delta_{\kappa} \phi|_{(x_0, y_0)} := (\nabla \cdot (\kappa \nabla \phi) + c\phi)|_{(x_0, y_0)} = (\kappa \Delta \phi + c\phi)|_{(x_0, y_0)}. \quad (2.11)$$

In this way, any grid functions of φ and f on the control volume may be utilized to describe the approximations the integral fluxes in (2.4) in the form of (2.8). Thus, the grid point spacings may not need necessarily to be uniform and can be adaptively determined locally. As a result, any desired quadrature points about the centroid may be included in the approximation of the flux integrals to discretize (2.4).

To enable effective higher-order accuracies, the Cauchy-Kovalevskaya procedure [14] is applied to replace higher order derivatives of φ in the expansions (2.9) and (2.10) by lower order derivatives of the local source term f. Thus, coefficients such φ_{xxxy} , φ_{xyyy} , φ_{xxxx} , etc in (2.9) and (2.11) are replaced by f_x , f_y , f_{yy} , f_{xx} , etc in order to more accurately represent the physics of the problem in the local expansions. As a result, the source term derivatives are introduced into (2.9) through higher-order derivatives of the equation (2.11) given as

$$-\kappa(\phi_{xx} + \phi_{yy}) + c\phi = f,$$

$$-\kappa(\phi_{xxx} + \phi_{xyy}) + c\phi_x = f_x,$$

$$-\kappa(\phi_{xxy} + \phi_{yyy}) + c\phi_y = f_y,$$

$$-\kappa(\phi_{xxxy} + \phi_{xyyy}) + c\phi_{xy} = f_{xy},$$

$$-\kappa(\phi_{xxxx} + \phi_{xxyy}) + c\phi_{xx} = f_{xx},$$

$$-\kappa(\phi_{xxyy} + \phi_{yyyy}) + c\phi_{yy} = f_{yy}, \text{ etc.}$$

The local equation error expansion E_{Qh} is described using the weighted quadrature approximations of the local fluxes by

$$E_{Q_h}(\phi) = -\kappa(\phi_0) \sum_{\partial \mathbf{Q}_h} W_i (\phi_i - \phi_0) - \sum_{\mathbf{Q}_h} w_i \phi_i - \sum_{\mathbf{Q}_h} v_i f_i, \neq 0$$
 (2.12)

where

$$\sum_{\partial \mathbf{Q}_h} W_i = 0, \quad \sum_{\partial \mathbf{Q}_h} w_i = 1, \quad \sum_{\mathbf{Q}_h} v_i = 1. \tag{2.13}$$

such that the differential and integral operator properties of the equations are preserved about each centroid. This error expansion measures the sum of the discrepancies of all possible flux formulation of (2.1) on the control volume. Thus, the formulation (2.4) offers a more complete accounting of local fluxes than traditional finite difference approximations which is a parameterized version of this framework.

To obtain the specifics the discretization for (2.1), the discrete minimax approach is utilized to determine the quadrature weights to annihilate the leading terms of the error expansion hierarchically. That is, the weights W_i , w_i , and v_i are determined to annihilate the leading terms of the error expansion of (2.5) and to further regulate the growth of the residual error. One advantage here is that for various innovative ways [18,29] to incorporate local micro scale properties into the numerical model, our comprehensive approach is naturally efficient in determining the right sampling and collocations of the source required for effective and robust higher-order accuracy.

Discretization of Helmholtz Equations in 2D

In this section, we demonstrate the advantages of the finite volume method described in Section 2 in developing consistent higher-order accurate schemes for the Helmholtz equation

$$-\Delta u - k^2 u = q \quad \text{in } \Omega, \tag{3.1}$$

where q is a given source function with compact support, $\Omega \subset {}^2$ is a bounded domain, $k = \omega/c$ is the wave number with ω and c as the circular frequency and speed of light respectively.

Many application problems in science including acoustic wave scattering from submarines, noise reduction in silencers and mufflers, earthquake wave propagation and others [17] are governed by the Helmholtz equation. The quality of the numerical solutions of the Helmholtz equation depends significantly on the size of the wavenumber k [4,17,19,31]. Our goal in developing higher-order accurate schemes for (3.1) is to demonstrate the pollution effect [31] in the local equation error expansion as well as the effectiveness of our approach in reducing the pollution effects to improve the qualities of the numerical solutions.

Consider the local approximation φ of u about the centroid of the control volume Q_h in two dimensions such that

$$-\Delta \varphi - k^2 \varphi = f, \tag{3.2}$$

where k is the wave number and $f: \mathbb{R}^2 \to \mathbb{C}$ is a local source term with local compact support defined according to (2.9) and (2.10) such that

$$\lim_{(x,y)\to(x_0,y_0)}\phi(x,y)=u(x_0,y_0)\quad\text{and}\lim_{(x,y)\to(x_0,y_0)}f(x,y)=q(x_0,y_0).$$

We describe the approximation of balanced flux integral form of the Helmholtz equation (3.1) about the centroid of the control volume O_h in two dimensions by

$$-\sum_{i=1}^{8} W_i \nabla \phi_i - \sum_{i=0}^{8} w_i \, \phi_i = \sum_{i=0}^{8} V_i f_i$$
(3.3)

and the local equation error expansion E_{Qh} by

$$E_{Q_h}(\phi) = -\sum_{\partial \mathbf{Q}_h} W_i \left(\phi_i - \phi_0\right) - \sum_{\mathbf{Q}_h} w_i \phi_i - \sum_{\mathbf{Q}_h} V_i f_i \tag{3.4}$$

where

$$W_0 = \sum_{i=1}^8 W_i, \quad w_0 = (1 - \sum_{i=1}^8 w_i)k^2, \quad V_0 = 1 - \sum_{i=1}^8 V_i$$
(3.5)

As discussed above, the source function approximations f_i on the control volume are defined specifically for the Helmholtz equation (3.2) by

$$f(x_0 + x, y_0 + y) = -(\triangle + k^2)\phi(x_0 + x, y_0 + y)$$
(3.6)

such that

$$f_0 = f(x_0, y_0) = -\phi_{xx}(x_0, y_0) - \phi_{yy}(x_0, y_0) - k^2 \phi(x_0, y_0)$$

which is consistent at the centroid of the control volume.

By substituting (2.9) and (3.6) into (3.4), the leading terms of the local equation error expansion are sorted to display the leading coefficients as functions of the weight parameters. The weight parameters are then determined to annihilate the leading coefficients sequentially. After eliminating the leading terms up to the third order terms, the weights are determined as

$$W_{0} = \frac{10}{3h^{2}}, \quad W_{1} = W_{3} = W_{5} = W_{7} = -\frac{2}{3h^{2}}, \quad W_{2} = W_{4} = W_{6} = W_{8} = -\frac{1}{6h^{2}},$$

$$v_{0} = \frac{2}{3} + 4v_{4}, \quad v_{1} = v_{3} = v_{5} = v_{7} = \frac{1}{12} - 2v_{4}, \quad v_{2} = v_{6} = v_{8} = v_{4}$$

$$w_{0} = (\frac{5}{6} - 2w_{5})k^{2}, \quad w_{1} = w_{3} = w_{7} = w_{5}k^{2}, \quad w_{2} = w_{4} = w_{6} = w_{8} = (\frac{1}{24} - \frac{w_{5}}{2})k^{2},$$

$$(3.7)$$

and the associated equation error residual is obtained as

Local Truncation Error =
$$T_4h^4 + T_6h^6 + T_8h^8 + O(h^{10})$$
 (3.8)

where

$$T_{4} = -\frac{k^{2}}{240}(k^{2}\triangle\phi + \triangle f) + k^{2}(\frac{1}{45} - \frac{w_{5}}{2})\frac{\partial^{4}\phi}{\partial x^{2}\partial y^{2}} + (v_{4} - \frac{1}{90})\frac{\partial^{4}f}{\partial x^{2}\partial y^{2}} + \frac{1}{240}(\frac{\partial^{4}f}{\partial x^{4}} + \frac{\partial^{4}f}{\partial y^{4}}),$$

$$T_{6} = \frac{11k^{4}}{60480}(k^{2}\triangle\phi + \triangle f) + \frac{k^{4}}{24}(w_{5} - \frac{19}{315})\frac{\partial^{4}\phi}{\partial x^{2}\partial y^{2}} - \frac{11}{60480}(k^{2}(\frac{\partial^{4}f}{\partial x^{4}} + \frac{\partial^{4}f}{\partial y^{4}}) - \frac{\partial^{6}f}{\partial x^{6}} - \frac{\partial^{6}f}{\partial y^{6}})$$

$$+ \frac{k^{2}}{24}(v_{4} - \frac{29}{420})\frac{\partial^{4}f}{\partial x^{2}\partial y^{2}} + \frac{1}{12}\left(v_{4} - \frac{5}{1008}\right)\left(\frac{\partial^{6}f}{\partial x^{4}\partial y^{2}} + \frac{\partial^{6}f}{\partial x^{2}\partial y^{4}}\right) + \frac{1}{3024}\frac{\partial^{8}\phi}{\partial x^{4}\partial y^{4}},$$

$$T_{8} = -\frac{13k^{6}}{3628800}(k^{2}\triangle\phi + \triangle f) + \frac{k^{6}}{720}(\frac{17}{252} - w_{5})\frac{\partial^{4}\phi}{\partial x^{2}\partial y^{2}} - \frac{13k^{4}}{2628800}(\frac{\partial^{4}f}{\partial x^{4}} + \frac{\partial^{4}f}{\partial y^{4}})$$

$$+ \frac{k^{4}}{720}(\frac{61}{840} - w_{5})\frac{\partial^{4}f}{\partial x^{2}\partial y^{2}} + \frac{k^{2}}{144}(\frac{73}{6300} - \frac{w_{5}}{10} - v_{4})\frac{\partial^{8}\phi}{\partial x^{4}\partial y^{4}}$$

+Higher order derivatives of f.

As clearly illustrated by the local truncation error (3.8), any selections of w_5 and v_4 subject to (3.5) guarantee fourth order accuracy mathematically. For $v_4 = 0$ and $w_5 = \frac{1}{12}$, the resulting scheme uses a 5-point stencils for the discretizations of k^2u and f and a 9-point stencil for the diffusion [12,23,25]. As indicated by (3.8), the mass and the stiffness matrices still depend on w_5 and v_4 respectively and their stabilities [11] may be further determined to optimize the scheme for a uniform of fourth-order accurate convergence. Furthermore, as illustrated by T_4 , T_6 , and T_8 in (3.8) which are polynomial functions in k, the numerical accuracies of the resulting schemes are significantly affected for high values k.

It is clear from the last terms in T_6 and T_8 that a larger twenty-five point control volume is needed to achieve beyond a sixth-order accuracy. In fact, a tenth-order accuracy can easily be achieved for interior grid points on the computational domain with twenty-five point control volumes. Now, in order to computationally achieve the order of accuracy of the schemes for high values of k, we must discretize and $absorb \triangle \phi$ and Δf in T_4 , T_6 and T_8 into the scheme and also choose w_5 as $w_5 = \frac{2}{45}$. As a result, the size of the leading term of the error may not be much affected by large values of the wave number k, and thus render the scheme to be consistently fourth-order accurate for moderate sizes of k.

Pollution Effects Reductions in Fourth-Order Accurate Schemes

As illustrated by (3.8), the tuncation error terms are polynomial functions of k with the same degree as h. The basic polynomial

$$P_E = A_p k^4 \triangle \phi + B_p k^2 \triangle f + C_p k^2 \frac{\partial^4 \phi}{\partial x^2 \partial y^2} + D_p \frac{\partial^4 f}{\partial x^2 \partial y^2}$$

$$\tag{4.1}$$

appears in T_4 , in T_6 multiplied by k^2 , and in T_8 multiplied by k^4 , and so on. Furthermore, the couplings get more complicated with additional derivative terms in higher order terms beyond h^4 as indicated by T_6 , T_8 , and therefore the source of associated pollution effects and drag on numerical accuracies and convergence for large values of k. Thus, the pollution effects cannot be eliminated in numerical computations since terms

like $\frac{\partial^8 \phi}{\partial x^4 \partial y^4}$ as in T_6 and T_8 require a larger computational stencil. However, the pollution effects can be

reduced on the 9-point stencil and our strategy is to resolve the terms $^{\triangle\phi}$, $^{\triangle f}$, $^{\frac{\partial^4\phi}{\partial x^2\partial y^2}}$ and $^{\frac{\partial}{\partial x^2\partial y^2}}$ that are coupled with k in the truncation error. For instance, the compact differencing of the Laplacians of φ and f on the control volume are given by

$$h^{4}\triangle\phi = -h^{2}\frac{20\phi_{0} - (\phi_{2} + \phi_{4} + \phi_{6} + \phi_{8}) - 2(\phi_{3} + \phi_{1} + \phi_{3} + \phi_{7})}{6} + \frac{1}{12}(k^{2}\triangle\phi + \triangle f)h^{6}$$

$$-\frac{1}{360}(k^{4}\triangle\phi + k^{2}\triangle f + 2k^{2}\phi_{xxyy} + 4f_{xxyy} + f_{xxxx} + f_{yyyy})h^{8} + O(h^{10}) \qquad (4.2)$$

$$h^{4}\triangle f = -h^{2}\frac{20f_{0} - (f_{2} + f_{4} + f_{6} + f_{8}) - 2(f_{3} + f_{1} + f_{3} + f_{7})}{6}$$

$$-\frac{1}{12}(2f_{xxyy} + f_{xxxx} + f_{yyyy})h^{6} + O(h^{8}), \qquad (4.3)$$

which are used in resolving the couplings of k in the residual error.

We rewrite the new symmetric fourth-order scheme for (3.1) on the control volume after resolving the k couplings in T_4 as

$$\sum_{i=0}^{8} \alpha_i \phi_i = \sum_{i=0}^{8} \beta_i f_i + \text{Residual Error}$$
(4.4)

where

$$\alpha_{0} = \frac{10}{3h^{2}} - \frac{67k^{2}}{90} + \frac{17h^{2}k^{4}}{1512}, \quad \alpha_{1} = \alpha_{3} = \alpha_{5} = \alpha_{7} = -\left(\frac{2}{3h^{2}} + \frac{2k^{2}}{45} + \frac{11h^{2}k^{4}}{7560}\right)$$

$$\alpha_{2} = \alpha_{4} = \alpha_{6} = \alpha_{8} = -\left(\frac{1}{6h^{2}} + \frac{7k^{2}}{360} + \frac{41h^{2}k^{4}}{30240}\right),$$

$$\beta_{0} = \frac{2}{3} + 4\beta_{8} - \frac{h^{2}k^{2}}{72}, \quad \beta_{1} = \beta_{3} = \beta_{5} = \beta_{7} = \frac{1}{12} - 2\beta_{4} + \frac{h^{2}k^{2}}{360},$$

$$\beta_{2} = \beta_{6} = \beta_{8} = \beta_{4} + \frac{h^{2}k^{2}}{1440}.$$

$$(4.5)$$

The associated truncation error is then given as

Error =
$$\left\{ \left(\beta_4 - \frac{1}{90} \right) \frac{\partial^4 f}{\partial x^2 \partial y^2} + \frac{1}{240} \left(\frac{\partial^4 f}{\partial x^4} + \frac{\partial^4 f}{\partial y^4} \right) \right\} h^4 \\
\left\{ \frac{k^4}{6048} (k^2 \triangle \phi + \triangle f) - \frac{k^2}{6048} (\frac{4k^2 \partial^4 \phi}{\partial x^2 \partial y^2} - \frac{\partial^4 f}{\partial x^4} - \frac{\partial^4 f}{\partial y^4}) - \frac{11}{60480} (\frac{\partial^6 f}{\partial x^6} + \frac{\partial^6 f}{\partial y^6}) \right\} h^6 \\
\left\{ -\frac{k^2}{3024} \frac{\partial^4 f}{\partial x^2 \partial y^2} + \frac{1}{12} \left(\beta_4 - \frac{5}{1008} \right) \left(\frac{\partial^6 f}{\partial x^4 \partial y^2} + \frac{\partial^6 f}{\partial x^2 \partial y^4} \right) + \frac{1}{3024} \frac{\partial^8 \phi}{\partial x^4 \partial y^4} \right\} h^6 \\
+ O(h^8) \tag{4.6}$$

where β_4 still remains a free parameter.

To improve consistency of the discretization furthermore, we apply (4.2) and (4.3) repeatedly to resolve the couplings in T_6 and T_8 after which the fourth-order scheme becomes

$$\sum_{i=0}^{7} \alpha_i u_i = \sum_{i=0}^{7} \beta_i f_i + \text{Truncation Error}$$
 (4.7)

where

$$\begin{array}{lll} \alpha_0 & = & \frac{10}{3h^2} - \frac{67k^2}{90} + \frac{17h^2k^4}{1512} + \frac{83h^4k^6}{226800} + \frac{h^6k^8}{51840} \\ \alpha_1 & = & \alpha_3 = \alpha_5 = \alpha_7 = -\left(\frac{2}{3h^2} + \frac{2k^2}{45} + \frac{11h^2k^4}{7560} + \frac{h^4k^6}{56700} + \frac{h^6k^8}{259200}\right) \\ \alpha_2 & = & \alpha_4 = \alpha_6 = \alpha_8 = -\left(\frac{1}{6h^2} + \frac{7k^2}{360} + \frac{41h^2k^4}{30240} + \frac{67h^4k^6}{907200} + \frac{h^6k^8}{1036800}\right) \\ \beta_0 & = & \frac{2}{3} + 4\beta_4 - \frac{19h^2k^2}{1512} - \frac{187h^4k^4}{453600} - \frac{h^6k^6}{51840} \\ \beta_1 & = & \beta_2 = \beta_3 = 4 = \frac{1}{12} - 2w_8 + \frac{2h^2k^2}{945} + \frac{37h^4k^4}{907200} + \frac{h^6k^6}{259200}, \\ \beta_5 & = & \beta_6 = \beta_8 = \beta_4 + \frac{h^2k^2}{1440} + \frac{h^4k^4}{36288} + \frac{h^6k^6}{1036800}. \end{array}$$

The local truncation error is now described as

Local Error =
$$\hat{T}_4 h^4 + \hat{T}_6 h^6 + \hat{T}_8 h^8 + O(h^{10})$$
 (4.8)

with

$$\hat{T}_{4} = \left(\beta_{4} - \frac{1}{90}\right) \frac{\partial^{4} f}{\partial x^{2} \partial y^{2}} + \frac{1}{240} \left(\frac{\partial^{4} f}{\partial x^{4}} + \frac{\partial^{4} f}{\partial y^{4}}\right),$$

$$\hat{T}_{6} = \frac{k^{2}}{6048} \left(\frac{\partial^{4} f}{\partial x^{4}} - 2\frac{\partial^{4} f}{\partial x^{2} \partial y^{2}} + \frac{\partial^{4} f}{\partial y^{4}}\right) + \frac{11}{60480} \left(\frac{\partial^{6} f}{\partial x^{6}} + \frac{\partial^{6} f}{\partial y^{6}}\right)$$

$$+ \frac{1}{12} \left(\beta_{4} - \frac{5}{1008}\right) \left(\frac{\partial^{6} f}{\partial x^{4} \partial y^{2}} + \frac{\partial^{6} f}{\partial x^{2} \partial y^{4}}\right) + \frac{1}{3024} \frac{\partial^{8} \phi}{\partial x^{4} \partial y^{4}}$$

$$\hat{T}_{8} = \frac{k^{4}}{172800} \left(\frac{\partial^{4} f}{\partial x^{4}} + \frac{\partial^{4} f}{\partial y^{4}}\right) + \frac{17k^{2}}{907200} \frac{\partial^{8} \phi}{\partial x^{4} \partial y^{4}}$$

+Higher order derivatives of f.

Pollution Effects and Computational Accuracy

In this section, we demonstrate the effects on computational accuracies and convergence rates for the different fourth-order accurate schemes described in Section 4 due to different levels of reductions of incidences of k in the local truncation error. In this regard, we compare the convergence rates of the schemes (3.7), (4.4), and (4.7) which are all mathematically fourth order accurate but have different leading terms in the residual errors due k.

To demonstrate convergence rate consistencies and quality of numerical solutions for moderate sizes of the wave number k, we consider the exact solution to the Helmholtz equation (3.1) to be

$$u(x,y) = \sin(w_1y + w_2x^2) + \sin(w_3x + w_4y^2)$$
(4.9)

which may be described as superposition of two waves. The source function which is also a superposition of four waves is determined as

$$f(x,y) = (4w_2^2x^2 + w_1^2 - k^2)\sin(w_1y + w_2x^2) + (4w_4^2x^2 + w_3^2 - k^2)\sin(w_3y + w_4x^2)$$

$$-2w_2\cos(w_1y + w_2x^2) - 2w_4\cos(w_3y + w_4x^2). \tag{4.10}$$

The source function is much more complex with larger amplitudes depending on the frequencies of the source waves where part of the waves are out of phase with the rest.

Consider the numerical error e(h), defined as the l^{∞} norm of the difference between the numerical solution φ and the exact solution u(x,y) of the Helmholtz equation (3.1). The convergence rate r is expressed such that

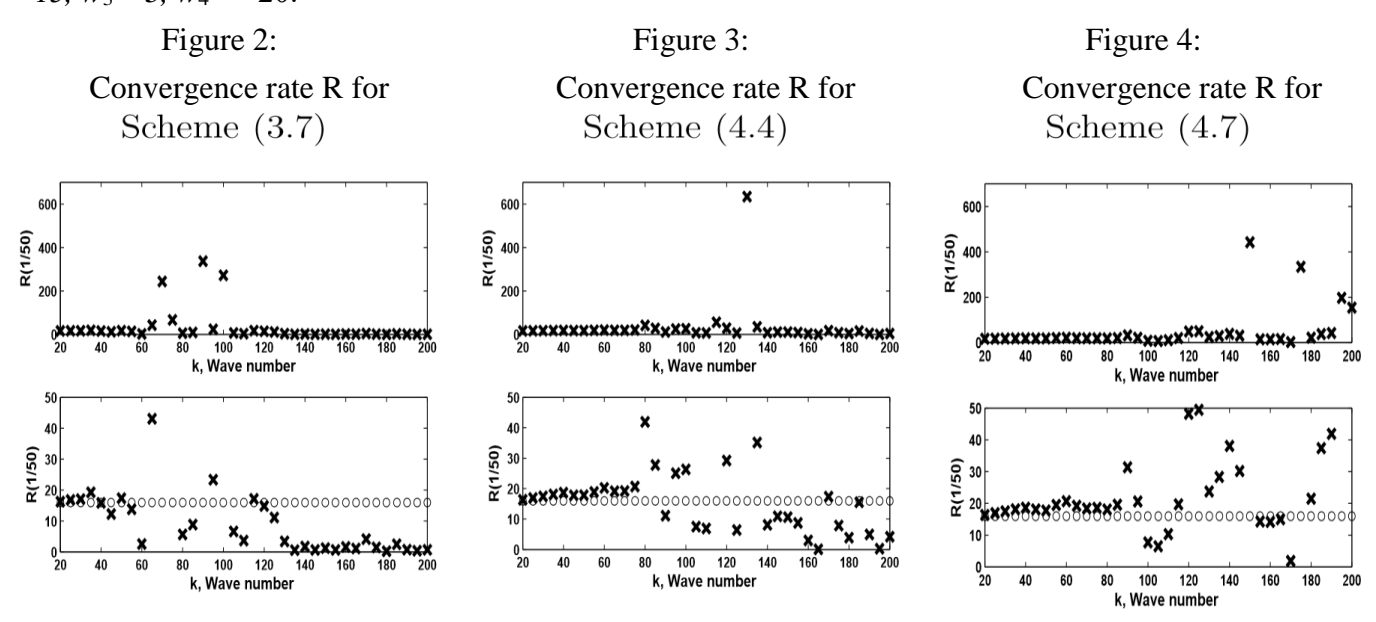
$$e(h) = ||u(x, y) - \phi_h||$$

= $Ch^r + o(h^r)$ as $h \to 0$ (4.11)

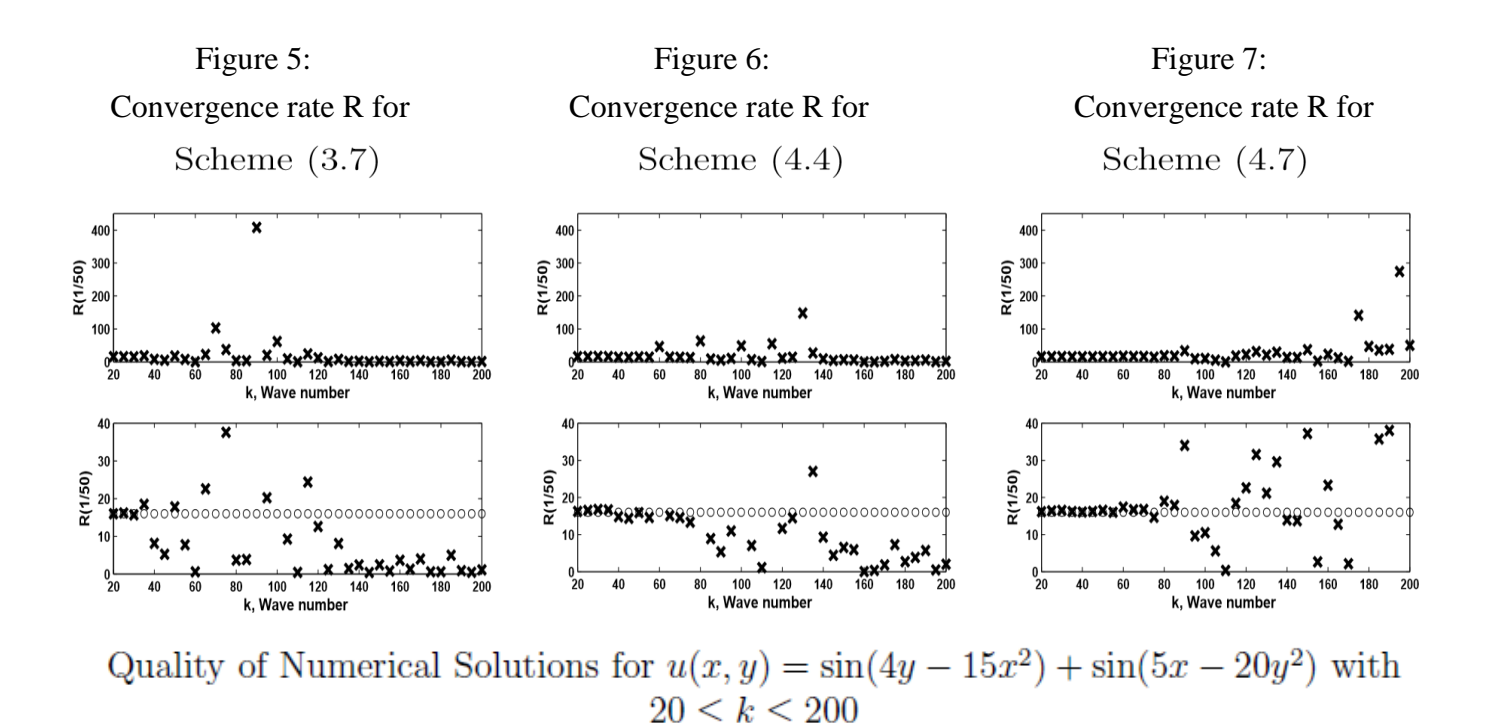
where *C* is independent of the grid size *h*. For a sufficiently small *h* we have that $e(h) \approx Ch^r$ for a numerical method of order *r* and hence $e(h/2) \approx C(h/2)^r$. Then the convergence rate through grid refinement analysis is defined by

$$R(h) = \frac{e(h)}{e(h/2)}$$
$$= 2^{r}.$$

To evaluate pollution effects due to k in the truncation error, we study the convergence rate R for grid resolutions $h = \frac{1}{50}$ and $h = \frac{1}{100}$ as the size of the wave number k is increased from 20 to 200. In Figures 2, 3, and 4, the convergence rates for the three schemes are displayed for the wave with frequencies $w_1 = 34$, $w_2 = -45$, $w_3 = 25$, $w_4 = -50$ and Dirichlet boundary conditions. The top rows show the complete picture of the distributions of R(1/50) and the second rows indicate the zoomed-in versions of the top rows. Figures 5, 6 and 7 illustrate similar convergence rate characterizations for the wave with frequencies $w_1 = 4$, $w_2 = -15$, $w_3 = 5$, $w_4 = -20$.



Quality of Numerical Solutions for
$$u(x,y) = \sin(34y - 45x^2) + \sin(25x - 50y^2)$$
 with $20 \le k \le 200$



The convergence rate patterns for the two waves $u(x,y) = \sin(34y-45x^2) + \sin(25x-50y^2)$ and $u(x,y) = \sin(4y-15x^2) + \sin(5x-20y^2)$ as displayed through Figures 2, 3, 4 and Figures 5, 6, 7 are similar for the three fourth-order accurate schemes 3.7, 4.4, and 4.7. Furthermore, the convergence rates for all the three schemes are uniformly fourth order accurate for $k \le 30$ as also indicated by the figures. However, between k = 30 and k = 110, the fourth-order convergence rate for scheme 3.7 cannot be guaranteed to be uniform and solution quality breaks down beyond k = 110. Scheme 4.4 is uniformly fourth-order accurate for $k \le 80$ and solution quality breaks down beyond k = 140. Scheme 4.7 is uniformly fourth-order accurate for $k \le 90$ and solution quality breaks down beyond k = 200 when pollution level in the $O(h^{10})$ term and beyond dominate the error. Thus, as the polluting term P_E described in (4.1) is resolved from the truncation error terms, quality of numerical solution improves. Clearly, the approach serves to demonstrate how to improve convergence sensitivities of numerical modeling to physical phenomena governed by partial differential equations.

Sixth-Order Schemes

In this section, we discuss sixth-order accuracy for (3.1) on the nine-point compact control volume. From the truncation error terms in (4.8), the numerical approximation of the fourth order derivatives of the source term are needed as indicated in [22] in order to annihilate \hat{T}_4 in (4.8) to ensure sixth-order accuracy.

It is clear from (4.7) that a larger computational stencil like a twenty-five point stencil is needed in order to extend to a tenth-order accuracy. For a given source term f, the last degree of freedom is selected as

 $\beta_4 = \frac{1}{90}$ and in order to annihilate T_4 , a second order approximation for $\frac{\partial^4 f}{\partial x^4} + \frac{\partial^4 f}{\partial y^4}$ given below

$$\frac{1}{15} \left(4f_{\frac{1}{2}} - 12f_0 - (f_1 + f_3 + f_5 + f_7) \right) = -\frac{h^4}{240} \left(\frac{\partial^4 f}{\partial x^4} + \frac{\partial^4 f}{\partial y^4} \right) - \frac{h^6}{5760} \left(\frac{\partial^6 f}{\partial x^6} + \frac{\partial^6 f}{\partial y^6} \right) + O(h^8)$$
(4.12)

is needed. When the above result (4.12) is incorporated in (4.7) and (4.8) with $\beta_4 = \frac{1}{90}$, sixth order accuracy is guaranteed.

For very high frequency regimes, the repeated use of (4.12) as indicated by the truncation error (4.8) is needed to reduce the size of the computational error as indicated in Tables 3 and 4.

Numerical Experiments

Several numerical tests have been performed to validate the effectiveness of this finite volume method for developing efficient, stable and consistent schemes for the Helmholtz equations on uniform mesh points. Pollution effects associated with high wave numbers has been demonstrated where the numerical schemes become more efficient for moderate sizes of the wave number for a given resolution as more truncation error terms coupled with *k* are determined and resolved.

We present some of the results of our tests to illustrate fourth- and sixth-order order accuracies for the schemes on a rectangular domain with Dirichlet boundary conditions.

The errors e(h) are measured with 1^{∞} norm according to (4.11) and the order of accuracy or convergence rate r is expressed such that for a constant C independent of h we have

$$r = \frac{\log(\frac{e(h_1)}{e(h_2)})}{\log(\frac{h_1}{h_2})} \tag{5.1}$$

where h_1 and h_2 are the grid spacings due to any two errors [25] measured according to (4.11)

We have demonstrated in Section 4.1 the need to resolve the terms $\triangle \phi$, $\triangle f$, $\frac{\partial^4 \phi}{\partial x^2 \partial y^2}$, and $\frac{\partial^4 f}{\partial x^2 \partial y^2}$ coupled with k in the truncation error for the nine-point compact control volume in order to ensure uniformly convergent schemes for the Helmholtz equation. So we present some of the numerical results for the scheme (4.7) through the following examples:

Example 1.

Consider the exact solution to the Helmholtz equation as

$$u(x,y) = \exp(xy)$$

where the corresponding source term is determined as

$$f(x,y) = -(x^2 + y^2)\exp(xy) - k^2 \exp(xy)$$

with k as the wave number. We present grid refinement analysis for this example in Table 1 to illustrate pollution effects associated with high wave numbers.

Table 1: Fourth order grid refinement analysis for $u(x, y) = \exp(xy)$ for Scheme (4.7)

h	$ u - \phi_h _{\infty}$ $k = 10$	cvge. rate	$ u - \phi_h _{\infty}$ $k = 50$	cvge. rate	$ u - \phi_h _{\infty}$ $k = 100$	cvge. rate
1/16	$5.980e^{-06}$		$1.188e^{-06}$		$1.023e^{-05}$	
1/32	$3.686e^{-07}$	4.02	$7.838e^{-08}$	3.92	$2.180e^{-07}$	5.55
1/64	$2.296e^{-08}$	4.00	$4552e^{-09}$	4.11	$7.527e^{-09}$	4.86
1/128	$1.430e^{-09}$	4.00	$2793e^{-010}$	4.03	$8.100e^{-10}$	3.22

Clearly, convergence is uniformly fourth-order accurate for k = 10 and k = 50 but not as uniform for k = 100 for this example as has been demonstrated for example (4.9) in Figures 4 and 7.

Example 2.

Consider the exact solution to the Helmholtz equation to be (4.9) whose source term is given by (4.10). The exact solution here may be described as the superposition of two nonlinear waves whose maximum amplitude is 2. However, the source term may be seen as a superposition of four nonlinear waves with variable amplitudes and some of the waves being out of phase. Thus, the source term can be complex necessitating the use of (4.12) to demonstrate sixth-order accuracy.

Table 2: Fourth-order grid refinement analysis for $u(x,y) = \sin(4y - 15x^2) + \sin(5x - 20y^2)$ with (4.7)

h	$ u - \phi_h _{\infty}$ $k = 10$	cvge. rate	$ u - \phi_h _{\infty}$ $k = 50$	cvge. rate	$ u - \phi_h _{\infty}$ $k = 100$	cvge. rate
1/16	$5.511e^{-02}$		$4.639e^{-02}$		$3.329e^{-03}$	
1/32	$3.351e^{-03}$	4.04	$1.244e^{-03}$	5.22	$6.346e^{-04}$	2.39
1/64	$2.081e^{-04}$	4.01	$7.779e^{-05}$	4.00	$1.832e^{-05}$	5.11
1/128	$1.299e^{-05}$	4.00	$4.860e^{-06}$	4.00	$2.081e^{-06}$	3.14

Again, convergence is uniformly fourth-order accurate for k = 10 and k = 50 but not as uniform for k = 100 as has been demonstrated in Figure 7.

In Table 3, we demonstrate six-order convergence analysis for $u(x,y) = \sin(4y - 15x^2) + \sin(5x - 20y^2)$

Table 3: Sixth-order grid refinement analysis for $u(x,y) = \sin(4y - 15x^2) + \sin(5x - 20y^2)$

h	$ u-\phi_h _{\infty}$	cvge.	$ u-\phi_h _{\infty}$	cvge.	$ u-\phi_h _{\infty}$	cvge.
	k = 10	rate	k = 50	rate	k = 100	rate
1/16	$1.961e^{-04}$		$6.520e^{-05}$		$7.080e^{-04}$	
1/32	$2.958e^{-06}$	6.05	$8.910e^{-07}$	6.19	$2.382e^{-06}$	8.21
1/64	$4.581e^{-08}$	6.01	$1.348e^{-08}$	6.05	$4.157e^{-08}$	5.84
1/128	$7.145e^{-10}$	6.00	$2.097e^{-10}$	6.01	$6.385e^{-10}$	6.02

Again, convergence is uniformly sixth-order accurate for k = 10 and k = 50 but not as uniform for k = 100.

Example 3.

Lastly, we demonstrate the need to resolve the source term derivative $\frac{\partial^4 f}{\partial x^4} + \frac{\partial^4 f}{\partial y^4}$ in the truncation error terms coupled with k in order to improve computational accuracy and quality of the solution. For instance, with the wave number set at k = 500, and the exact solution as $u(x,y) = \sin(34y-45x^2)+\sin(25x-50y^2)$, there is a significant difference between when (4.12) is applied only in T_6 and when (4.12) is applied both T_6 and T_8 as indicated by the truncation error (4.8). We demonstrate such numerical results in Tables 4 and 5.

Table 4: Computational error with k = 500 when (4.12) is applied in \hat{T}_6 of (4.8)

Table 5: Computational error with k = 500 when (4.12) is applied in \hat{T}_6 and \hat{T}_8 of (4.8)

h	$ u-\phi_h _{\infty}$	cvge. rate
1/100	$9.6835e^{-02}$	
1/200	$3.0540e^{-03}$	4.987
1/400	$6.4445e^{-05}$	5.566

h		$\ u-\phi_h\ _{\infty}$	cvge. rate
1/1	00	$3.8605e^{-03}$	
1/2	00	$6.8845e^{-05}$	5.809
1/4	.00	$8.1239e^{-07}$	6.405

Results in Tables 4 and 5 clearly show that using (4.12) to resolve the source term derivative $\frac{\partial^4 f}{\partial x^4} + \frac{\partial^4 f}{\partial y^4}$ in the truncation error terms coupled with k has been significant for the quality of numerical solution.

Discussion of Results

The local truncation error for the schemes may be described as a power series about the centroid (x_0, y_0) of the control volume by

$$E(h,k) = \sum_{i=0}^{\infty} \{ T_K(\xi, \eta, k) + T_0(\xi, \eta) \} \left((\xi - x_0)^{p+2i} + (\eta - y_0)^{p+2i} \right), \tag{6.1}$$

where $|\xi - x_0| \le h$, $|\eta - y_0| \le h$, and p = 4 or p = 6 for the fourth and sixth order methods respectively. The term $T_0(\xi, \eta)$ represents the local truncation error for the associated Poisson equation which has been shown to computationally converge uniformly. The term $T_K(\xi, \eta, k)$ is due to the wave number k and is described as

$$T_K = (k)^{p+2n} \sum_{i=0}^{p+2n} \frac{C_i(\xi, \eta)}{k^{2i}}$$
(6.2)

where C_i is a combination of higher-order derivatives of the source term and the solution. As discussed above, the truncation error terms are partly populated by k which dominate and determine the sizes of the errors for high wave numbers. One suggested way to reduce the size of the pollution error [2,7] is to require that hk be maintained as a constant. For moderate sizes of k and limited resolutions of the P_E terms in T_K , uniform convergence rates for the resulting fourth-order schemes have been achieved for the Helmholtz equations.

From (4.6) and (6.2), one way for T_K to converge uniformly is to require the option of hk < 1 necessitating smaller grid sizes. However, this choice which results in large size system matrices is expensive and the other way is by higher-order methods as illustrated above where the P_E terms are resolved as much as possible. The level of this reduction is limited by the number of grid points represented on the control volume. For a nine-point compact control volume, $\frac{\partial^8 \phi}{\partial x^4 \partial y^4}$ in T_6 and beyond cannot be resolved which puts a limitation on effective pollution effects reduction for high wave numbers. Therefore, for a given resolution of the control volume there is a limit on the size of the wave number for which consistency of the resulting schemes can be assured as illustrated in Section 4.1.

Conclusion

We have demonstrated the effectiveness of utilizing the finite volume discretization approach in developing new higher-order schemes for the Helmholtz equations with effective strategies for handling pollution effects associated with high wave numbers. In particular, pollution effects on convergence rates and quality of numerical solutions have been demonstrated. Using a more balanced flux integral formulation to construct an equation error expansion of the equation, a minimizing quadrature of local compact grid points are found for the discretization which further provides a more complete description and hence optimization of the pollution effects for improved quality of solutions. The fact that pollution effects associated with Helmholtz equations cannot be eliminated but may be reduced to obtain improved quality of solutions for moderate sizes of the wave number has also been demonstrated. Thus, this approach further serves to formulate a framework for improving sensitivities of higher-order numerical models for modeling physical phenomena.

References

- [1] I. M. Babuska and Ss A. Sauter, *Is the pollution effect of the fem avoidable for the helmholtz equation considering high wave numbers?*, SIAM Journal on Numerical Analysis **34** (1997), no. 6, 2392–2423.
- [2] G. Bao, G. W. Wei, and S. Zhao, *Numerical solution of the helmholtz equation with high wavenumbers*, Int. J. Numer. Meth. Engng **59** (2004), 389–408.
- [3] Q. Du, J. R. Kamm, R. B. Lehoucq, and M. L. Parks, *A new approach for a nonlocal, nonlinear conservation law*, SIAM J. APPL. MATH. **72** (2012), no. 1, 464–487.
- [4] H. C. Elman and D. P. OLeary, *Efficient Iterative Solution of the Three-Dimensional Helmholtz Equation*, J. Comput. Phys **142** (1998), 163–181.
- [5] Y. Fu, Compact fourth-order finite difference schemes for helmholtz equation with high wave numbers, **26** (2008), 98–111.
- [6] S. Gabersek and D. R. Durran, *Gap Flows through Idealized Topography. Part II: Effects of Rotation and Surface Friction*, J. Atmos. Sci. **63** (2006), 2720–2315.
- [7] F. Ihlenburg and I. Babuska, *Finite element solution of the Helmholtz equation with high wave number part i: the* h-version of the FEM., Comp. Math. Appl. **30** (1995),

9-37.

- [8] K. Ito, Y. Kyei, and Z. Li, *Higher-Order, Cartesian Grid Based Finite Difference Schemes for Elliptic Equations on Irregular Domains*, SIAM J. Sci. Comput. **27** (2005), 346–367.
- [9] P. Knabner and L. Angermann, *Numerical Methods for Elliptic and Parabolic Partial Differential Equations*, Springer-Verlag, New York, Inc, 2003.
- [10] Y. Kyei, Space-time finite volume differencing framework for effective higher-order accurate discretizations of parabolic equations, SIAM J. Sci. Comput. **34** (2012), no. 3, A1432–A1459.
- [11] Y. Kyei, J. P. Roop, and G. Tang, *A family of sixth-order compact finite difference schemes for poisson equation*, Adv. Numer. Anal. **Article ID 352174** (2010), 1–17.
- [12] S. K. Lele, Compact finite difference schemes with spectral-like resolution, J. Comput. Phys. **103** (1992), 1–42.
- [13] M. Li and T. Tang, A Compact Fourth-Order Finite Difference Scheme for Unsteady Viscous Incompressible Flows, J. Sci. Comput. **16** (2001), 29–45.
- [14] F. Lorcher, G. Gassner, and C. D. Munz, *An explicit discontinuous Galerkin scheme with local time-stepping for general unsteady diffusion equations*, J. Comput. Phys. **227** (2008), 5649–5670.
- [15] J. Ma, J. Zhu, and M. Li, *The galerkin boundary element method for exterior problems of 2-d helmholtz equation with arbitrary wavenumber*, Engineering Analysis with Boundary Elements **34** (2010), no. 12, 1058 1063.
- [16] W. H. Mason, *Applied computational aerodynamics*, Text/notes, http://www.dept.aoe.vt.edu/maxon/Mason f/CAtextTop.html, 1997.
- [17] O. Z. Mehdizadeh and M. Paraschivoiu, *Investigation of a two-dimensional spectral element method for Helmholtz's equation*, J. Comput. Phys. **189** (2003), 111–129.

- [18] P. Ming and X. Yue, *Numerical methods for multiscale elliptic problems*, J. Comput. Phys. **214** (2006), 421–445.
- [19] J. T. Oden, S. Prudhomme, and L. Demkowicz, *A posteriori error estimation for acoustic wave propagation problems*, Archives of Computational Mechanics and Engineering **12** (2005), no. 4, 343–389.
- [20] M. Piller and E. Stalio, *Finite–volume compact schemes on staggered grids*, J. Comput. Phys. **197** (2004), 1064–1094.
- [21] J. Santos and P. de Oliveira, *A converging finite volume scheme for hyperbolic conservation laws with source terms*, J. Comput. App. Math. **111** (1999), 239–251.
- [22] I. Singer and E. Turkel, *High-order finite difference methods for the Helmholtz equation*, Comput. Methods Appl. Mech. Engrg. **163** (1998), 343–358.
- [23] _____, Sixth Order Accurate Finite Difference Schemes for the Helmholtz Equation, J. Comput. Acoustics 14 (2006).
- [24] W. F. Spotz and G. F. Carey, *A high-order compact Scheme for the Steady StreamFunction Vorticity Equations*, Int. J. Numer. Meth. Eng **38** (1995), 3497–3512.
- [25] J. C. Strikwerda, *Finite Difference and Partial Differential Equations*, Wadsworth & BrooksCole Advanced Books & Software, 1989.
- [26] H. Suna, N. Kanga, J. Zhang, and E. S. Carlson, *A Fourth Order Compact Difference Scheme on Face Centered Cubic Grids with Multigrid Method for Solving 2D Convection Diffusion Equation*, Mathematics and Computers in Simulation **63** (2003), 651–661.
- [27] A. K. Verma, S. M. Bhallamudi, and V. Eswaran, *Overlapping control volume method for solute transport*, J. Hydr. Engrg. **5** (2000), 308–316.
- [28] K. Wang and Y. S. Wong, *Is Pollution Effect of Finite Difference Schemes Avoidable for Multi-Dimensional Helmholtz Equations with High Wave Numbers?*, / Commun. Comput. Phys. **21**, 490–514.
- [29] E. Weinan and B. Engquist, *Multiscale Modeling and Computation*, Notices Of The AMS **50** (2003), no. 9, 1062–1070.
- [30] Y. S. Wong and G. Li, Exact finite difference schemes for solving helmholtz equation at any wavenumber, Int. J. OF NUMER ANAL AND MODELING, SERIES B 2 (2011), no. 2, 91–108.
- [31] A. Erlangga Y, C. Vuik, and C. W. Oosterlee, *On A Robust Iterative Method For Heterogeneous Helmholtz Problems For Geophysics Applications*, Int. J. Numer. Anal. Modeling **2** (2005), 197–208.